Fluctuations in complex networks with variable dimensionality and heterogeneity

H.-H. Yoo and D.-S. Lee*
Department of Physics, Inha University, Incheon 22212, Korea
(Received 28 December 2015; revised manuscript received 4 March 2016; published 23 March 2016)

Synchronizing individual activities is essential for the stable functioning of diverse complex systems. Understanding the relation between dynamic fluctuations and the connection topology of substrates is therefore important, but it remains restricted to regular lattices. Here we investigate the fluctuation of loads, assigned to the locally least-loaded nodes, in the largest-connected components of heterogeneous networks while varying their link density and degree exponents. The load fluctuation becomes finite when the link density exceeds a finite threshold in weakly heterogeneous substrates, which coincides with the spectral dimension becoming larger than 2 as in the linear diffusion model. The fluctuation, however, diverges also in strongly heterogeneous networks with the spectral dimension larger than 2. This anomalous divergence is shown to be driven by large local fluctuations at hubs and their neighbors, scaling linearly with degree, which can give rise to diverging fluctuations at small-degree nodes. Our analysis framework can be useful for understanding and controlling fluctuations in real-world systems.

DOI: 10.1103/PhysRevE.93.032319

I. INTRODUCTION

It has recently been of great interest how the global organization of interactions of constituents influences the system-level dynamical characteristics [1,2], such as stability [3], criticality [4], controllability [5], evolvability [6,7], and so on. In particular, the impact of the connection topology for synchronizing the activities and balancing the loads of elements has attracted much attention [8], as it underlies the stability of diverse networked systems including brain networks [9], internet traffic routing [10], electric power transmission [11–13], and parallel computing [14–17].

The total number of interacting pairs primarily determines a system's synchronizability: The more pairs are interacting for their synchronization, the better fluctuations can be suppressed in a system. Yet how much an increase of interacting pairs can enhance the synchronization of a system, especially of heterogeneous networks universally found in the architecture of biological, social, and economic systems [1], has not yet been characterized. Its investigation can help us understand the mechanism for the stable functionality of systems with link failures [3,18] and illuminate how the connectivity of real-world systems is determined under the competition between the contribution to synchronizability and the cost of establishing new interaction channels.

We study the fluctuation of loads assigned to the least-loaded nodes in the neighborhood of each randomly selected node, following the Family model [19], in scale-free (SF) networks [20]. Given the sparse connectivity of most real-world systems [1] and possible applications to damaged systems, we consider the largest-connected component (LCC) of SF networks with small link density as substrates. The LCC is expected to have the core elements, the robustness of which is essential for the operation of the whole system [3].

Our study shows that the spectral dimension and the heterogeneity of substrates determine the scaling behavior of the load fluctuation. For weakly heterogeneous networks, the fluctuation in the LCCs first diverges with their size but later becomes finite while the link density is increased, which is shown to be related to the spectral dimension of the substrates increasing and passing the critical dimension 2 as predicted by the linear diffusion model. Therefore a finite link density, as large as the threshold, is sufficient for achieving synchronization. On the other hand, in strongly heterogeneous systems featured by lots of hubs, the load fluctuation is found to diverge with substrate size over a wide range of link density. We show that such anomalous divergence originates in large local fluctuations at abundant hubs and their neighbors, characterized by manifestions of the load fluctuation in star graphs. The condition for local hub-generated fluctuations to dominate the global fluctuation is presented in terms of the degree-dependent local fluctuations. These findings lead to a new framework of analyzing fluctuations in complex systems.

II. MODEL AND SCALING BEHAVIORS OF LOAD FLUCTUATIONS

Let us consider a network of N' nodes, their accumulated work loads $\{h_i\}$ of which evolve with time t following the Family model [19,21–23] as follows:

(i) A node i is selected randomly.

(ii) If $h_i \leqslant h_j$ for all neighbor nodes j of i, then $h_i \to h_i + 1$; otherwise, $h_\ell \to h_\ell + 1$ at a neighbor node ℓ having the smallest load among the neighbors.

(iii) Time t is increased by 1 after repeating (i) and (ii) N' times.

Assigning a new unit of load to the locally least-loaded node as above helps synchronize loads. For the substrates, the static model [24] is used to generate SF networks of N nodes, L links, and a power-law degree distribution $P_{\rm deg}(k) \sim k^{-\gamma}$ for k large with γ the degree exponent. The link density K is defined as $K \equiv L/N$. The obtained networks can be fragmented and we run the Family model on the LCC, consisting of N_G nodes and L_G links. The structure of the LCC varies with the link density K and the degree exponent γ of the original SF network (see Appendix A).

*deoksun.lee@inha.ac.kr

For the LCCs of SF networks with the link density $1/8 \leqslant K \leqslant 1$, the degree exponent $\gamma = 100, 3.6$, and 2.4, and different numbers of nodes N, we obtain in simulations the average size N_G of the LCCs and the load fluctuation $W(t) \equiv \sqrt{\langle (1/N_G)\sum_{i=0}^{N_G-1}(h_i(t)-\bar{h}_t)^2\rangle}$ with $\bar{h}_t = \sum_i h_i(t)/N_G$. We are interested in the time-averaged stationary-state fluctuation $W_{\rm sat} = \sqrt{\frac{1}{T-t_c}\sum_{t>t_c}^{T} W(t)^2}$ where T is the simulation time period and t_c is the crossover time after which $W(t)$ stops increasing and becomes stationary [25].

The simulation results for $(N_G, W_{\rm sat}^2)$ are presented in Fig. 1(a). For $\gamma = 3.6$ and $100, W_{\rm sat}$ increases with N_G when the link density K is small, but $W_{\rm sat}$ remains constant against increasing N_G for large K, suggesting that the addition of links should facilitate synchronization by preventing fluctuations from diverging with the substrate size. For $\gamma = 2.4, W_{\rm sat}$ increases with N_G for all considered K's. The scaling exponent α characterizing the divergence or finiteness of the load fluctuation as

$$W_{\rm sat} \sim N_G^{\alpha} \tag{1}$$

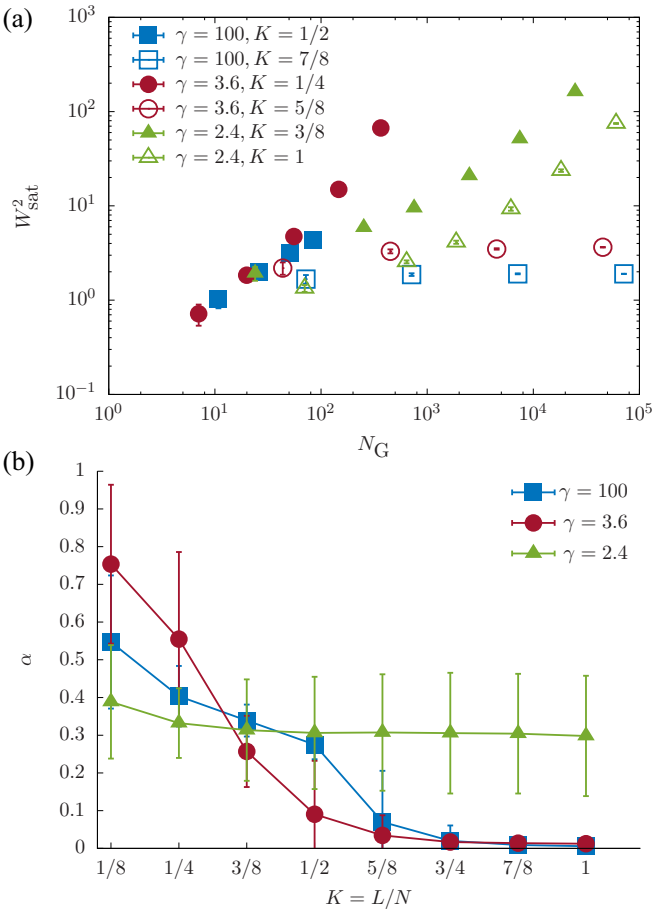

FIG. 1. Scaling of the stationary-state load fluctuation $W_{\rm sat}$ with respect to the average size N_G of the LCCs of SF networks with different link densities $K = L/N$ and degree exponents γ in the Family model. (a) Plots of $W_{\rm sat}^2$ vs N_G for selected K and γ. Error bars show the maximal difference between $W^2(t)$ and $W_{\rm sat}^2$. (b) Scaling exponents α in Eq. (1) as a function of K. Variations with the fitting range are represented by error bars (Appendix B).

can be a measure of synchronizability: Fluctuations will be finite in the thermodynamic limit ($N_G \to \infty$) if $\alpha = 0$ while it will diverge if $\alpha > 0$. The scaling behavior in Eq. (1) has been extensively studied in the context of surface growth on the Euclidean lattices [25], but that on complex networks is little understood [14,15,21–23].

The fluctuation exponent α decreases to reach zero within error bar at $K_{\rm th}$ between 1/2 and 5/8 for $\gamma = 100$ and $K_{\rm th}$ between 3/8 and 1/2 for $\gamma = 3.6$ [Fig. 1(b)]. These thresholds are close to the threshold K_c for the emergence of the giant component, the LCC of $N_G = O(N)$: $K_c \simeq 0.50$ for $\gamma = 100$ and $K_c = 0.31$ for $\gamma = 3.6$ [26]. The smaller threshold for $\gamma = 3.6$ than for $\gamma = 100$ implies that hubs are helpful for maintaining synchrony with small link densities. In contrast, for $\gamma = 2.4$, the scaling exponent α rarely decreases with K, remaining positive: Adding links, up to $K = 1$, hardly improves synchronizability. Therefore hubs may be hindering synchronization in this case. Similarly a logarithmic divergence of $W_{\rm sat}$ has been reported for the unfragmented configuration-model SF networks with the minimum degree $2, \gamma = 2.5$, and $K \simeq 2.4$ [21].

III. SPECTRAL DIMENSION OF SUBSTRATES

To understand the origins of these rich behaviors of $\alpha(K,\gamma)$, we first refer to the Edwards-Wilkinson (EW) model [27], a solvable linear diffusion model known to belong to the same universality class as the Family model on the Euclidean lattices. The time evolution of work loads in the EW model is represented by the EW equation $\frac{\partial h_i}{\partial t} = -\sum_{j=1}^{N'} M_{ij} h_j + \xi_i(t)$ for a network of N' nodes, where $\xi_i(t)$ is an uncorrelated noise and M_{ij} is the Laplacian matrix $M_{ij} = k_i \delta_{ij} - A_{ij}$ with A_{ij} the adjacency matrix. This is another mechanism of synchronizing the work loads at neighboring nodes, via linear coupling, and its lattice version has each randomly selected node i increase or decrease its load by 1 with equal probability as long as its new load would not differ from that of any neighbor node by more than 1 [25].

One can see from the corresponding Fokker-Planck equation that the load distribution takes the Gaussian form $P(\{h\}) \propto \exp[-(1/2)\sum_{ij} h_i M_{ij} h_j]$ in the stationary state, which leads to the analytic expression for the load fluctuation in the EW model, $W_{\rm sat}^2 = \frac{1}{N'}\sum_{n=2}^{N'} \frac{1}{\lambda_n}$ with λ_n's being the eigenvalues of the Laplacian matrix M sorted in the ascending order, and the smallest eigenvalue $\lambda_1 = 0$ [28]. The sum is dominantly governed by the small eigenvalues, the spectral density function of which, $\rho(\lambda) = (1/N')\sum_{n=2}^{N'} \delta(\lambda - \lambda_n)$, behaves in general as $\rho(\lambda) \sim \lambda^{d_s/2-1}$ for λ small with d_s the spectral dimension [29]. Using the spectral density function $\rho(\lambda)$, one can evaluate $W_{\rm sat}^2$ as

$$W_{\rm sat}^2 = \int_{\lambda_2} d\lambda\, \rho(\lambda)\, \lambda^{-1} \sim \int_{\lambda_2} d\lambda\, \lambda^{\frac{d_s}{2}-2} \sim \begin{cases} \lambda_2^{\frac{d_s}{2}-1} & \text{for} \quad d_s < 2, \\ \text{constant} & \text{for} \quad d_s > 2, \end{cases} \tag{2}$$

with λ_2 being the second smallest eigenvalue. In the LCC of size $N' = N_G$,λ_2 behaves as

$$\lambda_2 \sim N_G^{-\frac{2}{d_s}}, \tag{3}$$

from the extreme-value relation $\int_{\lambda_2} d\lambda\, \rho(\lambda) = \frac{N_G - 1}{N_G}$ [30]. Inserting Eq. (3) into Eq. (2), we find that $W_{\rm sat}$ follows Eq. (1) with [31]

$$\alpha^{(\rm EW)} = \begin{cases} \frac{1}{2}\left(\frac{2}{d_s} - 1\right) & \text{for} \quad d_s < 2, \\ 0 & \text{for} \quad d_s > 2. \end{cases} \tag{4}$$

We remark that the return-to-origin probability in random walks is related to the spectral density function by the Laplace transform [31].

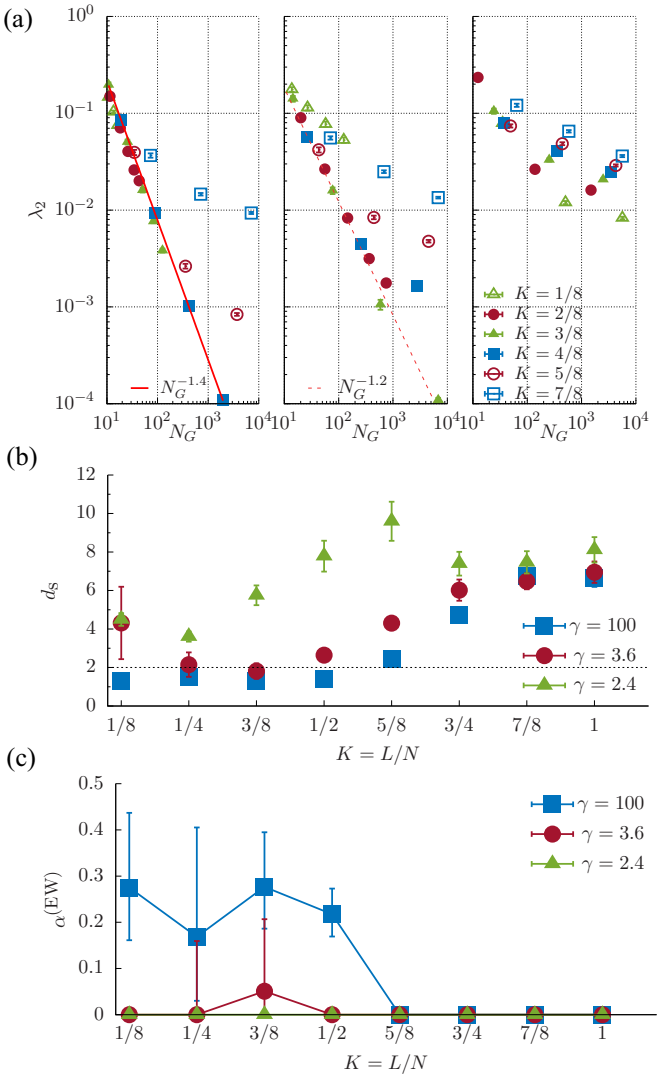

FIG. 2. Spectral dimension of the studied substrates. (a) The second smallest eigenvalue λ_2 of the Laplacian for $\gamma = 100$ (left), 3.6 (middle), and 2.4 (right). $\lambda_2 \sim N_G^{-1.4}$ best fits the data for $K = 1/2$ and $\gamma = 100$ and $\lambda_2 \sim N_G^{-1.2}$ for $K = 3/8$ and $\gamma = 3.6$. Error bars indicate the standard deviation of λ_2 over different realizations of networks. (b) Spectral dimensions d_s estimated by fitting Eq. (3) to the data in panel (a). The line is for $d_s = 2$. (c) $\alpha^{(\rm EW)}$ obtained by inserting the estimated d_s in Eq. (4).

To see whether Eq. (4) explains the behaviors of α in the Family model, we obtain numerically λ_2 [Fig. 2(a)] and determine d_s by fitting Eq. (3) to the obtained data. The spectral dimensions less than 2 appear for $K \leqslant 1/2$ and $\gamma = 100$ and for $K = 3/8$ and $\gamma = 3.6$ as shown in Fig. 2(b). As a result, for $\gamma = 3.6$, $\alpha^{(\rm EW)}$ obtained by using the estimated d_s in Eq. (4) is zero for $K \leqslant 1/4$, positive for $K = 3/8$, and again zero for $K \geqslant 1/2$. For $\gamma = 100$, $\alpha^{(\rm EW)} > 0$ for $K \leqslant 1/2$ and $\alpha^{(\rm EW)} = 0$ for $K > 1/2$. $\alpha^{(\rm EW)} = 0$ for all K and $\gamma = 2.4$. See Fig. 2(c). $\alpha^{(\rm EW)}$ transits from positive to zero between $K = 1/2$ and $5/8$ for $\gamma = 100$ and between $K = 3/8$ and $1/2$ for $\gamma = 3.6$, as does α in Fig. 1(b). This agreement suggests that the transitions of α from positive to zero arise from d_s of the LCCs increasing beyond 2.

For the LCCs of $d_s > 2$, however, the EW model prediction fails to explain all the Family model results. While $\alpha^{(\rm EW)} = 0$

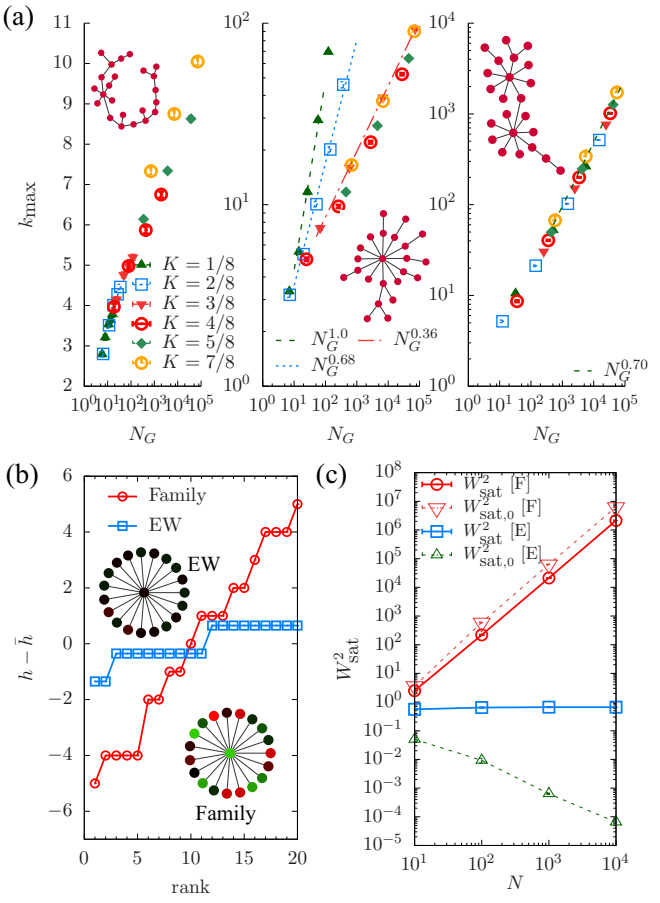

FIG. 3. Properties of the LCCs and the load fluctuations in star graphs. (a) The largest degree $k_{\max}$ scaling with the size N_G for $\gamma = 100$ (left), 3.6 (middle), and 2.4 (right). $k_{\max} \sim N_G^{\frac{1}{\gamma-1}}$ [26] except for $k_{\max} \propto N_G$ with $K = 1/8$ and $k_{\max} \sim N_G^{0.68}$ with $K = 1/4$ in the case of $\gamma = 3.6$. Insets: Examples of the LCCs for $K = 1/8$. (b) Sorted relative loads $h_r - \bar{h}$ vs their ranks r on the star graph of $N = 20$ nodes. Inset: Node color varies with the relative load $h - \bar{h}$ from red ($h - \bar{h} = -5$) through black ($h - \bar{h} = 0$) to green ($h - \bar{h} = 5$). (c) $W^2_{\rm sat}$ and the local fluctuation at the node in the center $W^2_{\rm sat,0}$ vs the size N in star graphs for the Family model ([F]) and the EW model ([E]).

for all the substrates with $d_s > 2$, α of the Family model is zero only for $K > K_{\rm th}$ with $\gamma = 3.6$ and 100; α is quite large for very small link densities $K \leqslant 1/4$ with $\gamma = 3.6$ and α remains positive for all K with $\gamma = 2.4$. These differences may be attributed to the nonlinear terms in the time-evolution equation of the Family model on heterogeneous networks [22]. The nonlinear terms are, however, hard to analyze further to gain insight into the origin of such different load fluctuations between the two models. Instead, we investigate in the next section the fluctuations in star graphs, as the heterogeneity of SF networks stem from the inclusion of many such star graphs of widely different sizes.

IV. FLUCTUATIONS IN STAR GRAPHS AND DEGREE-DEPENDENT LOCAL FLUCTUATIONS

A hub and its nearest neighbors form a star graph, which features the LCCs exhibiting $\alpha^{(\rm EW)} = 0$ ($d_s > 2$) but $\alpha > 0$. In Fig. 3(a), the LCC with $\gamma = 3.6$ and $K = 1/8$ is dominated by a single big star graph and has its largest degree $k_{\rm max} \propto N_G$ as the star graphs. The LCCs with $\gamma = 2.4$ has multiple star graphs.

On star graphs, loads are unevenly distributed in the Family model while they are almost uniform in the discrete EW model [Fig. 3(b)]. The hub node in the center is given a higher chance to increase its load than its neighbors, resulting in its load higher than the average in the Family model [23]. The peripheral nodes of degree 1 then have quite heterogeneous loads such that when sorted, loads increase linearly with their ranks [Fig. 3(b)]. As a result, $W_{\rm sat}$ increases linearly with the size N' [Fig. 3(c)]:

$$W_{\rm sat} \simeq c_{\rm star} N' \tag{5}$$

with $c_{\rm star} \simeq 0.2$.

Therefore the anomalously large exponent α for $\gamma = 3.6$ and $K = 1/8$ in Fig. 1(b) may stem from such large fluctuation around the hub as shown in the linear scaling in Eq. (5). The LCCs with $\gamma = 2.4$ can be viewed as multiple star graphs of different sizes that are interconnected [Fig. 4(a)]. This view leads us to understand the persistent divergence of $W_{\rm sat}$. To do so, we measure the stationary-state fluctuations of degree-k nodes $W_{\rm sat}(k) \equiv \sqrt{[1/(T-t_c)]\sum_{t>t_c}^{T}\langle\sum_{i=1}^{N_G}\delta_{k_i,k}[h_i(t)-\bar{h}_t]^2/\sum_{i=1}^{N_G}\delta_{k_i,k}\rangle}$, which would satisfy $W_{\rm sat} = \sqrt{\sum_k P_{\rm deg}(k) W_{\rm sat}(k)^2}$ if the ensemble variation of $P_{\rm deg}(k)$ is decoupled from that of $W_{\rm sat}(k)$. Our simulations for $K = 1$ and $N \leqslant 10^4$, all the substrates displaying $d_s > 2$, show that $W_{\rm sat}(k)$ decreases with k for k small but grows for k large as [Fig. 4(b)]

$$W_{\rm sat}(k) \simeq c_+ k^{\theta}. \tag{6}$$

The scaling exponent θ are estimated by fitting Eq. (6) to the data of $W_{\rm sat}(k)$, which remains around 1 for all K and $\gamma = 2.4$ and is about 0.8 for large K and $\gamma = 3.6$ [Fig. 4(c)]. For small K and $\gamma = 3.6$, θ display some fluctuation around 1 depending on the fitting range. These values of θ are reminiscent of the linear scaling in star graphs in Eq. (5), implying that the fluctuations at hubs of a given large degree is driven mainly by interacting with their neighbors. However, $c_+ \simeq 0.06$ in Eq. (6) is smaller than $c_{\rm star}$ in Eq. (5) and θ is smaller than 1 for $\gamma = 3.6$ as the embedded star graphs are not isolated in the substrates.

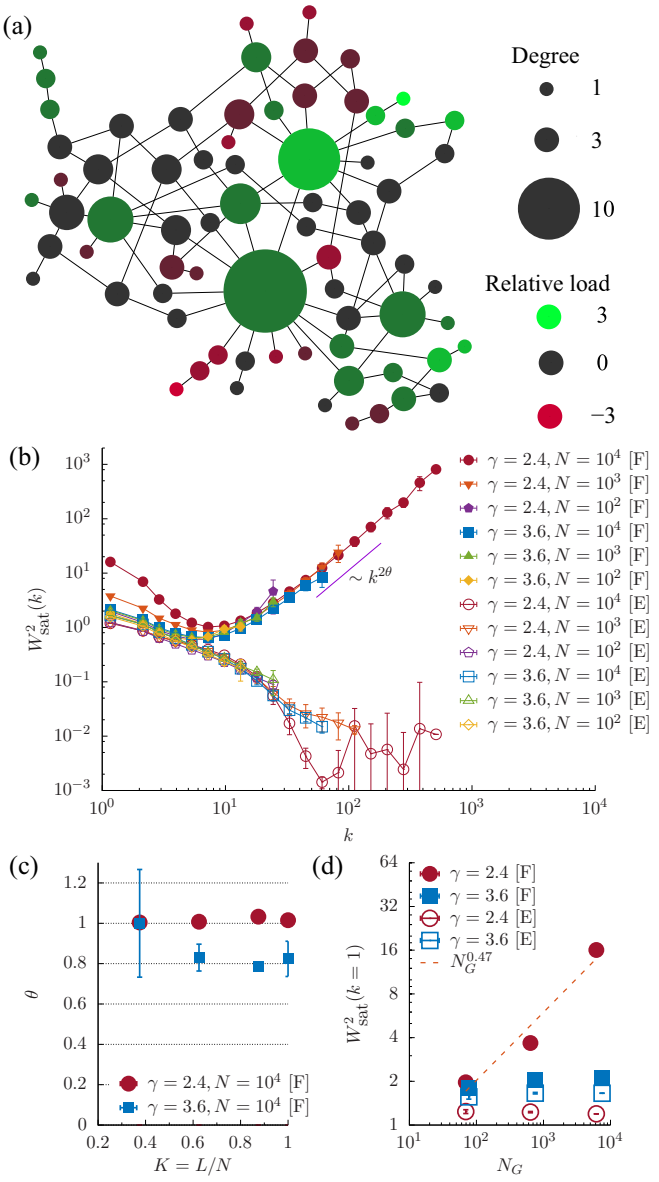

FIG. 4. Degree-dependent local fluctuations. (a) An LCC of $N_G = 72$ and $L_G = 95$ for $\gamma = 2.4$. Node color and size represent the degree k_i and the relative load $h_i - \bar{h}$. (b) $W_{\rm sat}(k)^2$ for $K = 1$ in the Family model ([F]) and the EW model ([E]). (c) Estimated scaling exponents θ in Eq. (6). (d) $W^2_{\rm sat}(k = 1)$ vs N_G. The line fits the data for $\gamma = 2.4$ in the Family model.

Summing up the fluctuations at hubs over different $k > k_c$ with k_c a characteristic degree, one can evaluate a part of the global fluctuation $W_+^2 \equiv \sum_{k>k_c} P_{\rm deg}(k) W_{\rm sat}(k)^2$ by using Eq. (6) as $W_+^2 \sim \sum_{k>k_c} k^{-\gamma} k^{2\theta}$, which diverges with the largest degree $k_{\rm max}$ as $W_+^2 \sim k_{\rm max}^{1-\gamma+2\theta}$ if $\gamma < 1 + 2\theta$, and is finite if $\gamma > 1 + 2\theta$. Inserting $k_{\rm max} \sim N_G^{\frac{1}{\gamma-1}}$, valid for most cases [Fig. 3(a)], we find that $W_+ \sim N_G^{\alpha_+}$ with

$$\alpha_+ = \begin{cases} \frac{\theta}{\gamma-1} - \frac{1}{2} & \text{for} \quad \gamma < 1 + 2\theta, \\ 0 & \text{for} \quad \gamma > 1 + 2\theta. \end{cases} \tag{7}$$

For $\gamma = 2.4$, $\alpha_+ \simeq 0.2$ with $\theta = 1$, which is close to α within error bar in Fig. 1(b) and is equal to α estimated for the data with $N \leqslant 10^4$ only. More importantly, Eq. (7) presents a plausible reason why the diverging fluctuations over a wide range of K appears exclusively for $\gamma = 2.4$ in our simulations: A sufficient number of hubs are needed to make the sum of their large fluctuations diverge with the substrate size. Note that the criterion $1 + 2\theta$ is 3 with $\theta = 1$. θ is negative in the EW model [31].

Small-degree nodes are connected to hubs by a link or a path, and can thus display large fluctuations as well. $W_{\rm sat}(k)$ for small k and $\gamma = 2.4$ increases with N_G as does W_+. In particular, for $k = 1$,

$$W_{\rm sat}(k = 1) \sim N_G^{\alpha_-} \tag{8}$$

with the exponent $\alpha_- \simeq 0.2 \pm 0.1$ [Fig. 4(d)], which agrees well with α_+ and α, suggesting that the large fluctuations at abundant hubs and their neighbors induce diverging fluctuations at small-degree nodes.

V. DISCUSSION

We have here shown that diverging fluctuations can be driven by either low dimensionality or strong heterogeneity, only the former of which has been well known for regular lattices but both of which are present in real-world complex systems. Our study illuminates the nature of the heterogeneity-driven fluctuations. Fluctuations around hubs, as in star graphs, are crucially dependent on the details of dynamics, as exemplified by the difference between the Family model

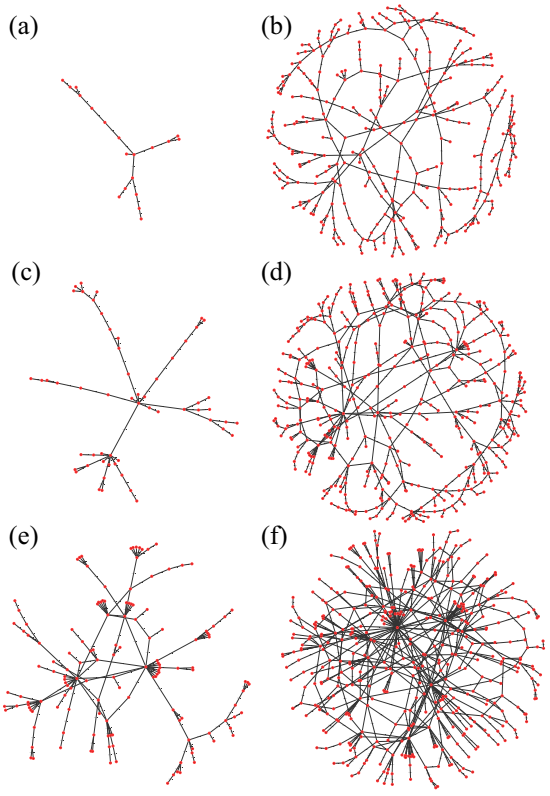

FIG. 5. Examples of the largest connected components (LCC) of SF networks. Those in panels (a), (c), and (e) are from the SF networks with link density $K = L/N = 1/4$ and those in panels (b), (d), and (f) are with $K = 5/8$. The degree exponent γ is 100 for panels (a) and (b), 3.6 for panels (c) and (d), and 2.4 for panels (e) and (f).

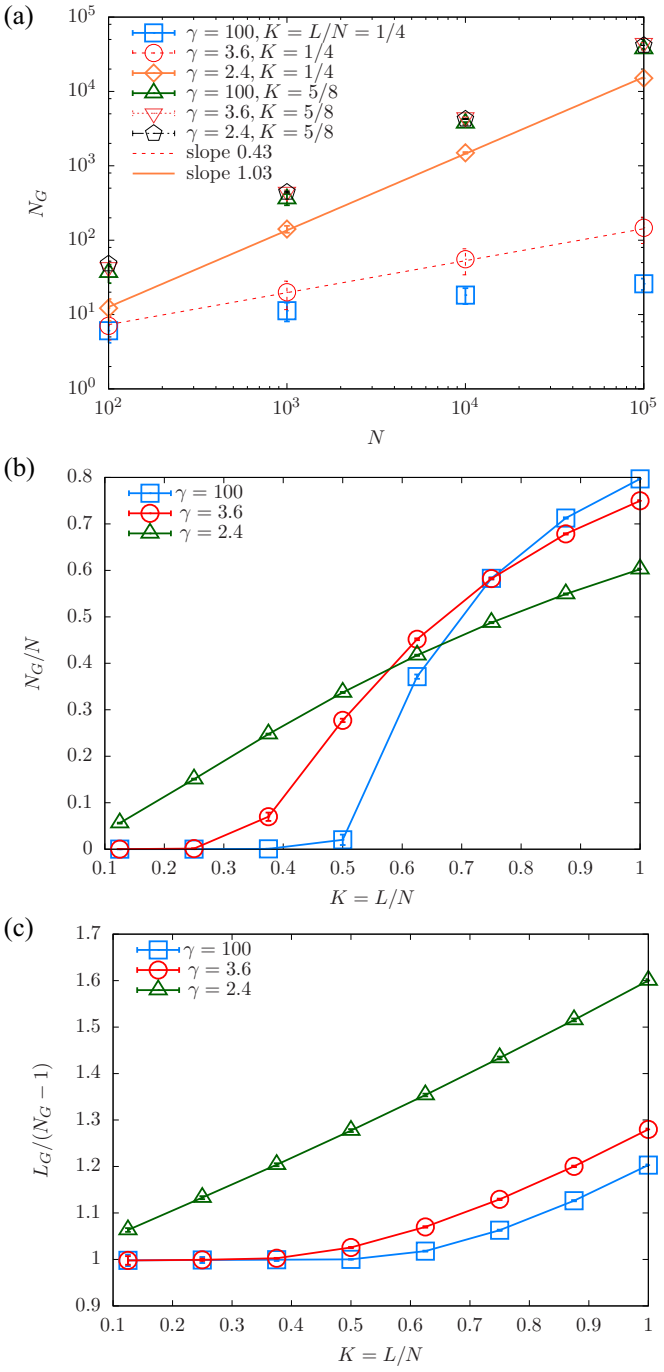

FIG. 6. Size and connectivity of the LCCs of SF networks. (a) The number of nodes N_G in the LCC. For $\gamma = 3.6$ and 100, N_G grows sublinearly with the total number of nodes N for small link density ($K = 1/4$) while it grows linearly for large link density ($K = 5/8$). $N_G \sim N^{0.43}$ for $\gamma = 3.6$ and $K = 1/4$ (dashed line) with the exponent close to $1/(\gamma - 1) = 0.39$ [26]. For $\gamma = 2.4$ and $K = 1/4$, $N_G \sim N^{1.03}$ (solid line). (b) Plots of N_G/N vs the link density $K = L/N$ for $N = 10^5$. (c) Plots of $L_G/(N_G - 1)$ vs K for $N = 10^5$. L_G is the number of links in the LCC. It remains 1 for small K and $\gamma = 3.6$ and 100 while it deviates from 1 even for small K and $\gamma = 2.4$.

and the EW model. Allowing work load to be assigned to a neighbor in the Family model gives hub nodes a higher chance to increase loads than small-degree nodes, causing the local fluctuation around hubs to increase linearly with their degrees. The sum of those local fluctuations can diverge when there are sufficiently many hubs, the condition of which we identified. In contrast, the local fluctuation at a hub decay with its degree in the EW model, preventing the global fluctuation from diverging solely due to the heterogeneity of substrates. This suggests that the synchronization of complex systems can be significantly affected by the details of dynamic processes. One of the implications of our study is that assigning jobs to neighbors should be supervised carefully in, e.g., the internet routing, parallel computing, and the electric power grids, so as not to lose the system's synchronization owing to diverging fluctuations.

Given the limitation of the system size in our simulations, it is desirable to further investigate the finite-size effects. As our study demonstrates, the spectral dimension, the fluctuation of the dynamic processes of interest on star graphs, and the degree-dependent local fluctuations can be measured and analyzed to help understand the empirical fluctuations in diverse systems.

ACKNOWLEDGMENTS

This work was supported by a National Research Foundation of Korea (NRF) grant funded by the Korean government (No. 2013R1A2A2A01068845) and the research fund (Grant No. 51906) of Inha University.

APPENDIX A: LCC OF THE STATIC-MODEL SF NETWORKS

The LCCs of SF networks with different link densities and degree exponents are presented in Fig. 5. For $\gamma > 3$, the number of nodes N_G in the LCC increases sublinearly with the total number of nodes N if the link density is small. If the link density is large, N_G grows linearly with N. See Fig. 6(a). If LCC is as large as of order N ($N_G = O(N)$), one can call it the giant component. In Ref. [26], it was shown for $\gamma > 3$ that the scaling behavior of N_G is changed from $O(N^{\frac{1}{\gamma-1}})$ to $O(N)$ at a critical threshold

$$K_c = \frac{(\gamma-1)(\gamma-3)}{2(\gamma-2)^2}, \tag{A1}$$

exactly at which N_G is $O(N^{\max\{\frac{2}{3},\frac{\gamma-2}{\gamma-1}\}})$. On the other hand, for $\gamma < 3, N_G$ scales linearly with N for all $K > 0$ as shown in Figs. 6(a) and 6(b) [26].

It is not only the size but also the topological structure of the LCC that changes with the link density K of the original network. For K small and $\gamma > 3$, the LCC takes a tree structure: The ratio $L_G/(N_G - 1)$ remains close to 1 [Fig. 6(c)], which is 1 if the network is of perfect tree structure without any loop. The ratio deviates from 1 and increases with K for K large, as loops are formed. The boundary of these distinct behaviors is K_c in Eq. (A1) [26]. For $\gamma < 3$, on the contrary, the ratio $L_G/(N_G - 1)$ increases almost linearly with the link density K, meaning that the LCC is loopy even with small link densities.

APPENDIX B: ESTIMATION OF THE SCALING EXPONENT α AND THE SPECTRAL DIMENSION d_s

The scaling exponent α in Fig. 1(b) is estimated by fitting Eq. (1) to the data points of $W_{\rm sat}$'s and N_G's, some of which are shown in Fig. 1(a), for given K and γ. Given the limitation that N_G is finite in our simulations and the finite-size effects indeed seen in our data in Fig. 1(a), we also compute the local exponents α in the ranges $N_G \in [N_1, N_2]$ as $\alpha(N_1, N_2) = \log \sqrt{\frac{W^2_{\rm sat}(N_2)}{W^2_{\rm sat}(N_1)}} / \log(\frac{N_2}{N_1})$, where N_1 and N_2 are the adjacent values of N_G considered in our simulations and take the maximal difference between $\alpha(N_1, N_2)$ and the estimated α as the error bar.

The spectral dimension d_s in Fig. 2(b) is estimated by fitting Eq. (3) to the data points of λ_2's and N_G's shown in Fig. 2(a), for given K and γ, and the error bars are determined in the same way as for α.

APPENDIX C: LAPLACIAN SPECTRA OF STAR GRAPHS

Note that $W_{\rm sat}$ is finite in the EW model on star graphs as the eigenvalues of the Laplacian are given by $\lambda_1 = 0, \lambda_2 = \lambda_3 = \cdots = \lambda_{N-1} = 1$ and $\lambda_N = N$, implying $d_s \to \infty$.

[1] R. Albert and A.-L. Barabási, Rev. Mod. Phys. **74**, 47 (2002).
[2] A. Barrat, M. Barthélemy, and A. Vespignani, *Dynamical Processes on Complex Networks* (Cambridge University Press, Cambridge, UK, 2008).
[3] R. Albert, H. Jeong, and A.-L. Barabási, Nature (London) **406**, 378 (2000).
[4] S. Dorogovtsev, A. Goltsev, and J. Mendes, Rev. Mod. Phys. **80**, 1275 (2008).
[5] Y.-Y. Liu, J.-J. Slotine, and A.-L. Barabasi, Nature (London) **473**, 167 (2011).
[6] A. Wagner, *Robustness and Evolvability in Living Systems* (Princeton University Press, Princeton, NJ, 2005).
[7] D.-S. Lee, Phys. Rev. E **90**, 052822 (2014).
[8] A. Arenas, A. Díaz-Guilera, J. Kurths, Y. Moreno, and C. Zhou, Phys. Rep. **469**, 93 (2008).
[9] E. Bullmore and O. Sporns, Nat. Rev. Neurosci. **10**, 186 (2009).
[10] L. Zhao, Y.-C. Lai, K. Park, and N. Ye, Phys. Rev. E **71**, 026125 (2005).
[11] R. Albert, I. Albert, and G. L. Nakarado, Phys. Rev. E **69**, 025103 (2004).
[12] M. Rohden, A. Sorge, M. Timme, and D. Witthaut, Phys. Rev. Lett. **109**, 064101 (2012).
[13] A. E. Motter, S. A. Myers, M. Anghel, and T. Nishikawa, Nat. Phys. **9**, 191 (2013).
[14] G. Korniss, M. A. Novotny, H. Guclu, Z. Toroczkai, and P. A. Rikvold, Science **299**, 677 (2003).

[15] B. Kozma, M. B. Hastings, and G. Korniss, Phys. Rev. Lett. **92**, 108701 (2004).
[16] Y. Kim, J.-H. Kim, and S.-H. Yook, Phys. Rev. E **83**, 056115 (2011).
[17] Y. Kim, I. Kwon, H. Chae, and S.-H. Yook, Phys. Rev. E **90**, 012814 (2014).
[18] B. Karrer, M. E. J. Newman, and L. Zdeborová, Phys. Rev. Lett. **113**, 208702 (2014).
[19] F. Family, J. Phys. A **19**, L441 (1986).
[20] A.-L. Barabási and R. Albert, Science **286**, 509 (1999).
[21] A. L. Pastore y Piontti, P. A. Macri, and L. A. Braunstein, Phys. Rev. E **76**, 046117 (2007).
[22] C. E. La Rocca, L. A. Braunstein, and P. A. Macri, Phys. Rev. E **77**, 046120 (2008).
[23] D. Torres, M. A. Di Muro, C. E. La Rocca, and L. A. Braunstein, EPL **110**, 66001 (2015).
[24] K.-I. Goh, B. Kahng, and D. Kim, Phys. Rev. Lett. **87**, 278701 (2001).
[25] A.-L. Barabási and H. Stanley, *Fractal Concepts in Surface Growth* (Cambridge University Press, Cambridge, UK, 1995).
[26] D.-S. Lee, K.-I. Goh, B. Kahng, and D. Kim, Nucl. Phys. B **696**, 351 (2004).
[27] S. F. Edwards and D. R. Wilkinson, Proceed. Royal Soc. A **381**, 17 (1982).
[28] S. Hwang, D.-S. Lee, and B. Kahng, Phys. Rev. E **90**, 043303 (2014).
[29] D. Ben-Avraham and S. Havlin, *Diffusion and Reactions in Fractals and Disordered Systems* (Cambridge University Press, Cambridge, UK, 2000).
[30] E. Gumbel, *Statistics of Extremes* (Columbia University Press, New York, 1958).
[31] S. Hwang, D.-S. Lee, and B. Kahng, Phys. Rev. E **90**, 052814 (2014).